SCHOOL OF ADVANCED STUDIES OF THE ROMANIAN ACADEMY

”ILIE MURGULESCU” INSTITUTE OF PHYSICAL CHEMISTRY

Discipline: CHEMISTRY

SYNTHESIS AND CHARACTERIZATION OF NEW ELECTRODE MATERIALS FOR ENERGY CONVERSION AND STORAGE SYSTEMS

PhD THESIS SUMMARY

PhD Supervisor:

Dr. Habil. SPĂTARU NICOLAE

PhD Student:

MIHAI MARIUS-ALEXANDRU

2025

CONTENTS

Keywords: electrode materials; energy conversion; energy storage; electrolysis; photoelectrolysis; supercapacitors

1. INTRODUCTION

The relentless exploitation of fossil fuels has caused a sharp increase in the concentration of greenhouse gases such as CO_2, CH_4, N_2O or water vapor [1], the global average temperature being approximately 1.1 °C higher than the pre-industrial period [2]. This phenomenon, known as *global warming*, can have the most severe consequences on the environment, as exceeding certain temperature thresholds can trigger irreversible and self-sustaining processes [3], endangering the planet's capacity to sustain life [1,3]. In this context, the *Paris Agreement* (2015) set the goal of keeping the global average temperature well below 2 °C and pursuing efforts to limit the increase to 1.5 °C [4]. To achieve this objective, the IEA (International Energy Agency**)** mandates the NZE (Net Zero Emissions by 2050) plan, which requires carbon dioxide emissions to be net-zero by the year 2050 [5]. Furthermore, fossil fuels are depletable resources, with an estimated period of approximately 100 years for coal and 50 years for natural gas and petroleum until their total consumption [6]. Therefore, it is necessary to find alternatives to fossil fuels. This can be achieved through *renewable energy sources*, but their intermittent nature requires the use of *energy storage systems* (ESS) [7].

Among the various energy storage systems, we will restrict our focus to electrochemical systems, particularly supercapacitors and water electrolysis cells, because through them, hydrogen can be obtained – a clean and very versatile fuel [8–11]. Having the highest energy density [12], hydrogen is considered a key factor in the transition to renewable sources and the fight against global warming [13].

Depending on the method of hydrogen production, a *color* or *flavor* is assigned (the *hydrogen rainbow*), with the hydrogen obtained through electrolysis powered by renewable energy being called *green hydrogen*.

Currently, there are several types of water electrolysis systems, which are classified according to their operating temperature, the state and pH of the electrolyte *etc.* The most important types of systems are *alkaline electrolyzers* (ALC, with a liquid alkaline aqueous

solution electrolyte, such as concentrated KOH or NaOH), *proton-exchange membrane electrolyzers* (PEM, with a solid polymer membrane electrolyte), and solid oxide electrolyzers (SO) [11]. Each one has its own advantages and disadvantages, according to its operating principle. Nevertheless, alkaline electrolyzers are considered very attractive due to their technological maturity and low manufacturing costs [11,14].

Although the thermodynamic limit cannot be surpassed, *i.e.*, the minimum voltage applied to the electrolysis cell (under normal conditions) must be at least 1.23V, a portion of the energy required for the electrolytic process can be supplied by solar light. This process is called *photo-assisted electrolysis* or *photoelectrolysis* [15–17].

The overall efficiency of the electrolytic process (conventional or photoassisted) is limited by the slow kinetics of the water oxidation half-reaction, thus largely depending on the ability of the (photo)anodes to catalyze this redox process [15,17–20]. Consequently, the present work primarily focuses on the design and study of new anodic materials using innovative and modern fabrication methods, while also considering the practicality and large-scale implementation potential of these materials. At the same time, a more comprehensive approach was pursued, combining the study of different elements so that the results obtained could offer a wider variety of solutions for the entire system, from the perspective of electrochemistry. Thus, this work is structured into three main parts, each addressing the improvement of essential components of a renewable energy conversion system:

Part I: Optimization of the Oxygen Evolution Reaction (OER) – *Thermally Interpenetrated Co–Ni Mixed Oxide as Efficient Oxygen Evolution Electrodes*. A new method for synthesizing Co- and Ni-based anodes is investigated. The objective is to obtain a unique atomic configuration, predicted to be robust and electrocatalytically active, through a controlled thermal interdiffusion treatment.

Part II: Improvement of WO_3-TiO_2 Photoanodes – *Enhanced photoelectrochemical activity of WO_3-decorated native titania films by mild laser treatment.* The study of anodic processes is explored in depth using the photoelectrolytic method. Hybrid photoanodes made of WO_3 deposited on a TiO_2 substrate (n-type semiconductors) are used and subjected to laser treatment. This treatment aims to improve the electrical contact at the semiconductor junctions and modify properties relevant to photoelectrocatalysis (*e.g.*, band structure, charge carrier recombination rate *etc.*).

Part III: Development of Electrodes for Supercapacitors - *Enhancement of the capacitive features of WO_3 supported on pristine and functionalized graphite by appropriate adjustment of the electrodeposition regime*. Since an integrated system requires a module capable of absorbing rapid voltage fluctuations (which the alkaline electrolyzer does not tolerate well [11]), and supercapacitors are ideal for this task (due to their high power density, long lifespan, high efficiency, and fast response [7]), the improvement of the capacitive properties of WO_3-based electrodes deposited on graphite substrates is being studied, by adjusting the electrodeposition regime and functionalizing the substrates.

3. EXPERIMENTAL PART

3.1. Thermally Interpenetrated Co–Ni Mixed Oxide as Efficient Oxygen Evolution Electrodes [21]

3.1.1. Introduction

Comparatively, the anodic reaction is much slower than the cathodic one, determining the overall efficiency of the electrolysis process [22–25]. The reference materials for oxygen evolution reaction (OER) electrodes are based on noble metals such as Ru, Ir, and especially their oxides (RuO_2 and IrO_2) [24]. Although these materials exhibit superior electrocatalytic activity in oxygen evolution in both acidic and basic media, their use is severely limited by their high cost, very low abundance, and a high rate of corrosion [25]. These drawbacks can be overtaken by using electrocatalysts based on common metals that can successfully accomplish the catalytic function for oxygen evolution in an energy-efficient manner. Many studies have been published in this regard, where various catalytic materials based on common metals such as High Entropy Alloys (HEA) [26], metal carbides [27], MXenes [28], perovskites [29], oxides, *etc.*, have been shown to exhibit quite high catalytic activities for oxygen evolution, although most of them are limited to alkaline media. However, because they are inexpensive, easy to synthesize, and robust, the traditional oxides [24,29–32], hydroxides, and oxyhydroxides [33,34] are still the subject of many studies concerning OER electrocatalysts. Also, a recent scientometric analysis shows that there has been a massive increase in the number of publications on metal oxide-based OER electrocatalysts since 2010 [35]. Among the most promising electrocatalytically active oxides and (oxy)hydroxides are

those of 3d transition metals, particularly cobalt [36] and nickel [37]. Moreover, by combining these two elements, a synergistic effect is expected, with beneficial consequences on catalytic activity [29,30]. The electrical conductivity of oxides and (oxy)hydroxides is rarely satisfactory, the potential drop caused by it inevitably leading to energy losses. Usually, carbon-based materials are mixed with the catalyst to eliminate this inconvenience [31], but these can corrode during the OER process [24,30,38]. Therefore, it is recommended to design electrocatalysts that simultaneously exhibit both increased catalytic activity and good electrical conductivity.

Given the increased OER activity of materials based on Co and Ni and their demonstrated synergistic effect, these elements were selected for the design of efficient and stable electrocatalysts. At the same time, the abundance of cobalt in the Earth's crust is at least three times lower than that of nickel [39]. Therefore, in this study, oxygen evolution electrodes were fabricated using microquantities of Co electrodeposited onto Ni substrates. After deposition, the samples were subjected to a thermal treatment intended to interpenetrate the metal atoms at the surface, resulting in an alloy of nanometric thickness. This was performed by heating the samples in an inert environment to temperatures exceeding the Tammann temperature (T_m), which is approximately ½ of the absolute melting temperature of a solid, a threshold above which atoms within a crystal lattice become mobile and can diffuse [40]:

$$x = 2\sqrt{D(T)\tau} \tag{3.1}$$

where D (T) ($cm^2\ s^{-1}$) is the diffusion coefficient as a function of the absolute temperature, T (K), x (cm) is the penetration depth, and τ (s) is the duration of the treatment. This preparation method should produce robust electrodes with minimal ohmic drop, as a thin and smooth transition is expected between the metallic substrate (Ni) and the catalytic surface (Co-Ni mixed oxide). Consequently, in addition to a more efficient use of Co resources, the method could also help reduce ohmic losses by avoiding the need to use thick, poorly conductive catalyst layers.

3.1.2. Materials and methods

3.1.2.1. Electrodes preparation

Pure nickel plates (5×20 mm^2) were cleaned and used as substrates for galvanostatic cathodic electrodeposition. Three distinct methods were applied to obtain electrodes with: microquantities of Co (μCoN), Ni:Co ≈ 1:2 alloy (NiCoN), or pure Co (CoN). Except one

μCoN sample, the electrodes obtained by electrodeposition were subjected to a thermal mixing treatment at 850 °C, in argon atmosphere, to form unique atomic configurations (*e.g.*, tm−μCoN). Finally, all samples (including a pure Ni reference) were calcined in air at 400 °C for surface oxidation, thus yielding the final materials (μCoNO, tm−μCoNO, tm−NiCoNO, tm−CoNO, NO) for electrochemical characterization.

3.1.3. Results and discussion

3.1.3.1. Cobalt microquantitative deposition and thermal mix treatment

Microquantitative metal electrodeposition generated Co nanoparticles on the surface of the Ni substrate (Figure 1). According to the particle size distribution (Figure 1d), the average diameter of the nanoparticles is approximately 145 nm. Therefore, the duration of the thermal treatment, *i.e.*, 200 s, was calculated (Eq. (3.1)) using this value ($D(T) = D_0 e^{(-\Delta H/RT)}$; D_0 = 1.11 cm^2 s^{-1} and ΔH = 64.9 kcal mol^{-1} [41]).

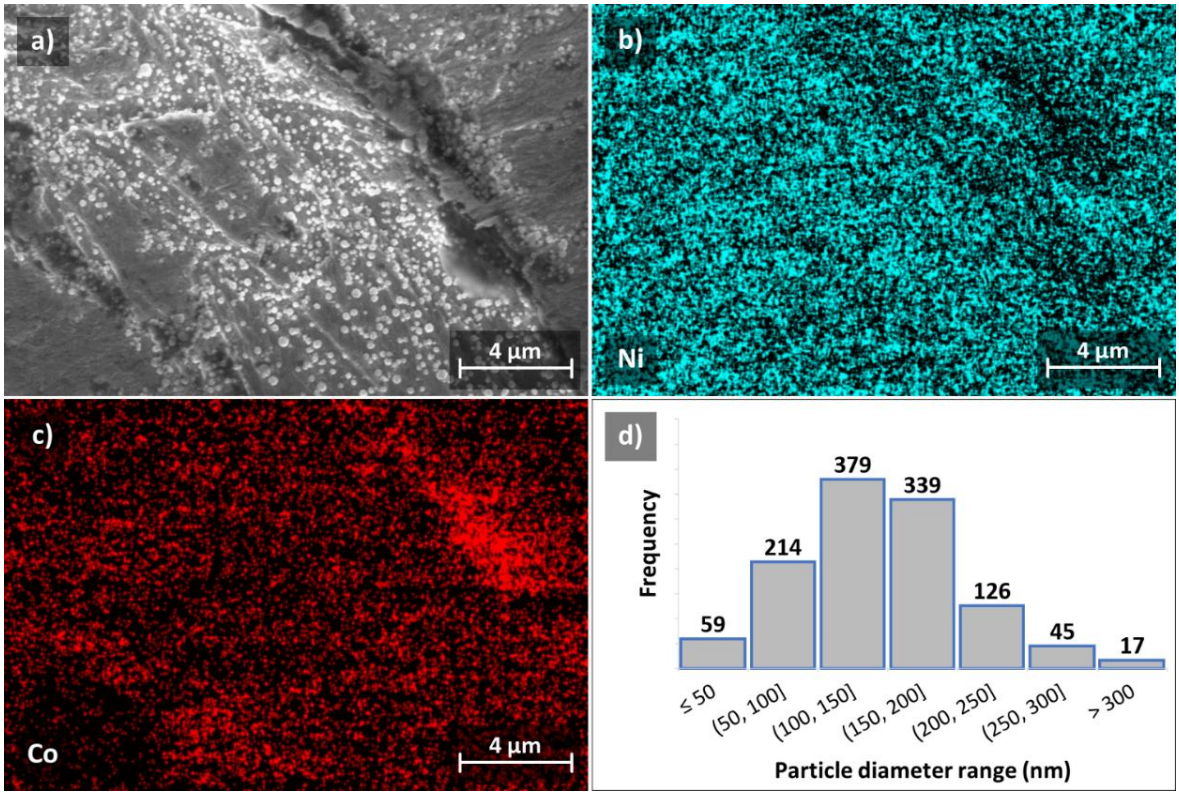

Figure 1. SEM image (a), EDX mapping of Ni (b) and Co (c) and Co particle size distribution (d) for the untreated, as-deposited μCoN sample

3.1.3.2. Electrochemical characterization, surface morphology, and electrocatalytic properties assessment

Cyclic voltammetry measurements confirmed that the tm−NiCoNO electrode exhibits a characteristic behavior of the $NiCo_2O_4$ mixed oxide [42,43]. The electrochemical behavior of the samples with micro-quantities of Co (μCoNO and tm−μCoNO) was intermediate and unique, suggesting the formation of new surface species that are not simple superpositions of NiO and Co_3O_4 binary oxides with the $NiCo_2O_4$ mixed one. As expected, mixed oxides demonstrated superior electrocatalytic activity compared to the simple reference oxides.

SEM and EDX analyses show clear differences between the thermally mixed and non-mixed samples (Figure 2 and Table 3.1). The thermally mixed electrode with microquantities of Co (tm−μCoNO) exhibited a uniform morphology and a homogeneous distribution of elements, indicating the complete absorption of Co into the Ni substrate and an increased resistance to oxidation (minimum O percentage). In contrast, the non-mixed electrode (μCoNO) had a complex/segregated morphology, with visible oxidized Co nanoparticles on the surface. These observations are supported by EDX data, where an uneven distribution was observed for the non-mixed sample, and the reduced percentage of Co in the thermally mixed sample confirmed atomic migration into the Ni volume. The thermally alloyed Ni−Co alloy electrode confirmed a homogeneous morphology, typical of an oxidized alloy.

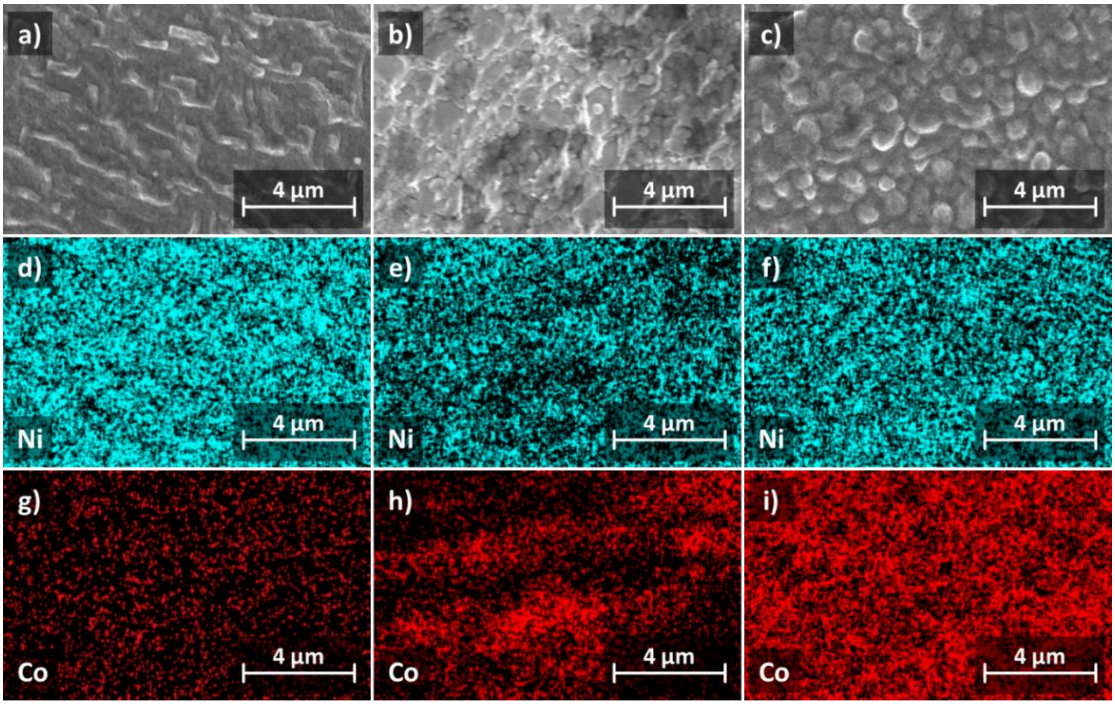

Figure 2. SEM (a-c) and EDX mapping (d-i) for tm-μCoNO (a, d, g), μCoNO (b, e, h), and tm-NiCoNO (c, f, i) electrodes samples.

Table 3.1. EDX relative elemental composition.

Electrode	Atomic percentage		
	Ni	Co	O
tm-μCoNO	91.68%	2.70%	5.62%
μCoNO	72.84%	6.27%	20.89%
tm-NiCoNO	23.76%	56.28%	19.97%

The electrocatalytic performance of the electrodes in the Oxygen Evolution Reaction (OER) was evaluated by Linear Sweep Voltammetry (LSV) and Tafel analysis. Among the tested electrodes, tm−μCoNO proved to be the most active electrocatalyst, recording lowest values for both onset potential (1.542 V) and the Tafel slope (36.47 mV dec^{-1}), being clearly superior to the μCoNO (1.577 V and 44.13 mV dec^{-1}) and tm−NiCoNO (1.590 V and 67.26 mV dec^{-1}) samples.

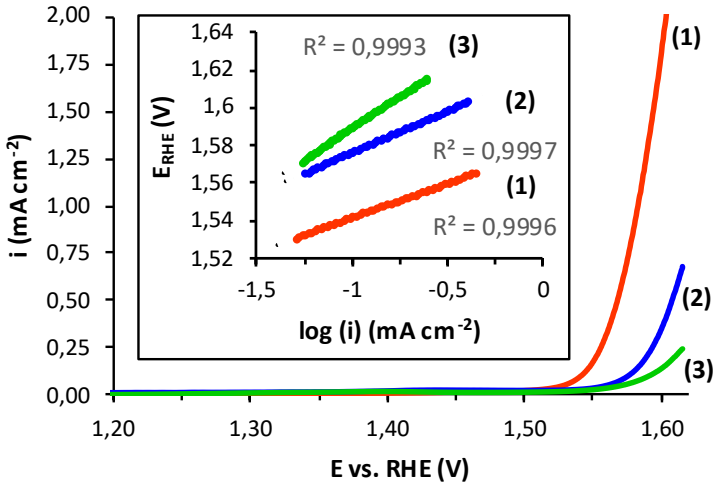

Figure 3. OER LSV curves (sweep rate, 5 mV s^{-1}) for tm-μCoNO (red line 1), μCoNO (blue line 2), and tm-NiCoNO (green line 3) alongside their Taflel plots (inset), in 0.1 M KOH.

Electrochemical Impedance Spectroscopy (EIS) measurements at the OER potential (1.57 V_{RHE}) were essential for the correct estimation of the Electrochemical Active Surface Area (ECSA) of the electrodes. This method is preferred over cyclic voltammetry because it better captures the actual surface properties during the reaction [44]. The resulting ECSA values are 2.20 cm^2 for tm−μCoNO, 2.25 cm^2 for μCoNO and 8.09 cm^2 for tm−NiCoNO. The minimum ECSA value of the tm-μCoNO electrode highlights that its superior performance results from the electrocatalytic centers generated by the thermal mixing treatment, rather than from a larger surface area. Furthermore, EIS revealed that the value associated with the solution resistance (R_s) was the lowest for the tm−μCoNO electrode (10.9

Ω vs. 12.2 Ω for μCoNO and 15.6 Ω for tm−NiCoNO). This finding confirms the oxidation resistance observed in the EDX data (R_s also includes the active film resistance, thus depends on its thickness).

3.1.3.3. Surface chemistry and correlation to catalytic properties

XPS (X-ray Photoelectron Spectroscopy) analyses were essential for correlating the surface chemistry with the electrocatalytic performance of the electrodes, highlighting different oxidation states and compositions for the tm−μCoNO, μCoNO, and tm−NiCoNO samples. Surprisingly, in the thermally mixed electrode case, tm−μCoNO (most active one), its surface was found to primarily exhibit metal elements not exceeding +2 oxidation state. The Co $2p_{3/2}$ (781.0 eV) and Ni $2p_{3/2}$ spectra (deconvolution) indicated the dominant presence of $Co(OH)_2$ and NiO. The O 1s spectra confirmed the presence of the lattice oxygen of NiO and $Co(OH)_2$. This configuration, which is resistant to oxidation (as previously observed by EDX), is considered the main reason for the increased electrocatalytic activity. In the case of the μCoNO electrode (non-mixed), the surface chemistry is complex and multiphasic, featuring multiple oxidation states, including Co^{3+} and Ni^{3+} species (most likely from a $NiCo_2O_4$ spinel-type structure), in addition to NiO and Co_3O_4. This result is consistent with the segregated morphology observed by SEM (islands of Co/mixed oxides on the Ni oxides substrate). The tm−NiCoNO electrode (thermally mixed alloy) exhibited spectra typical of a $NiCo_2O_4$ spinel structure, confirming the dominant presence of Co^{3+} and Ni^{2+}/Ni^{3+} species, also validating the cyclic voltammetry results. To conclude, the thermal interdiffusion treatment conferred oxidation resistance to the tm−μCoNO electrode, preventing spinel phase formation and leading to superior intrinsic catalytic activity in the OER, associated with the presence of $Co(OH)_2$/NiO.

3.1.3.4. Discussion

The superior catalytic performance of the tm−μCoNO electrode is primarily attributed to its strong oxidation resistance (confirmed by EDX and XPS), which maintains atomic species stability at the surface. The XPS analysis showed, surprisingly, that the Co atoms at the surface do not exceed +2 oxidation state ($Co(OH)_2$). This stabilization of Co^{2+} is facilitated by the surrounding abundance of NiO [45,46], a phenomenon that favors the formation of Co^{2+} species even at 400 °C (*vs.* 1000 °C). This oxidation state of Co is crucial, as it is considered the main active species in the Oxygen Evolution Reaction (OER). DFT theoretical studies [47] indicate that the involvement of the Co^{2+}/Co^{3+} redox couple leads to

lower overpotentials, a hypothesis experimentally confirmed [48–51]. From another perspective, one might assume that the thermal mixing treatment leads to the formation of isolated monomolecular species of Co_1O_x, which intensify the OER activity [52].

3.2. Enhanced photoelectrochemical activity of WO_3-decorated native titania films by mild laser treatment [53]

3.2.1. Introduction

Since Fujishima and Honda's revolutionary study [54], titanium dioxide (TiO_2) has been recognized for its stability and low cost in photoelectrocatalysis [55,56], although its efficiency is limited by the large band gap (~3.0 – 3.2 eV) and rapid recombination of charge carriers [57]. To overcome these limitations, various methods have been proposed, such as doping it with different nonmetals [58–62], applying thermal treatments to create oxygen vacancies (forming Ti^{3+}) [63,64], or surface modification with Au or Pt nanoparticles [65,66]. A promising method for increasing the efficiency of TiO_2-based photocatalysts is by coupling it with semiconductors like WO_3 (non-toxic, robust, with a smaller band gap [67]), whose band positions ensure a better separation of charge carriers [68]. Although most studies have focused on catalysts in powder form [69–71], attention is shifting toward immobilized, double-layer systems, and electrodeposition of WO_3 onto native (pristine) TiO_2 is considered an effective method for obtaining these layers [72]. Furthermore, a recent study shows that the charge carrier recombination rate can be significantly reduced by applying a mild laser treatment [73].

The purpose of this study is to obtain and evaluate the efficiency of WO_3-TiO_2 hybrid systems (formed by the electrodeposition of WO_3 onto native TiO_2), as well as to modify their surfaces by applying a mild laser treatment, intended to enhance the photoelectrocatalytic performance of these systems.

3.2.2. Material and methods

The TiO_2/Ti substrates are prepared by etching Ti samples (1 cm^2) in an oxalic acid solution at 80 °C [74,75], followed by the spontaneous formation of the pristine TiO_2 film upon exposure to air for 24 h. On this substrate, WO_3 is then electrodeposited by applying

consecutive potential pulses (1 s, from 0.1 V to -0.6 V), from an acidic Na_2WO_4 solution [76]. Finally, some of the WO_3-TiO_2/Ti samples are subjected to a mild laser treatment (1058 nm, 8W, 0.78 J cm^{-2} [73]), using a high linear speed (1 m s^{-1}) to avoid the oxidation of titanium [77], thus completing the preparation of the hybrid L−WO_3-TiO_2/Ti electrodes.

3.2.3. Results and discussion

Potentiodynamic measurements under intermittent UV light demonstrated that all WO_3-TiO_2 hybrid systems exhibited significantly higher photocurrents than pure TiO_2, displaying a photoanodic behavior characteristic of n-type semiconductors. This improvement is due to the formation of the WO_3-TiO_2 junctions; since the dark current remains unchanged, an increase in the active electrochemical surface area can be excluded. The photoelectrocatalytic efficiency depends on the amount of WO_3 deposited, reaching a maximum for a charge density of ∼70 mC cm^{-2}. An excessive amount of WO_3 decreases the activity, possibly by increasing the number of charge carrier recombination centers [78].

The morphological analysis (SEM) of the most active electrode (WO_3-TiO_2 at 40 mC cm^{-2}) revealed an irregular surface, with WO_3 clusters gathered around the sharp edges of the substrate (Figure 4a). Furthermore, the analysis of the WO_3 particle size distribution revealed that the average diameter is 110 nm, having the majority below 150 nm (∼70%).

The laser treatment applied to the WO_3-TiO_2 hybrid film induced essential microscopic changes, as seen in the SEM images (Figure 4b vs. Figure 4a). The applied fluence (0.78 J cm^{-2}), exceeding the ablation threshold, initiated a melting–solidification process, resulting in smoothing and rounding of the substrate surface, the direction of the beam scan being clearly visible (inset Figure 4b). A crucial aspect is the morphological reorganization: the initial groupings of WO_3 particles (red circles, Figure 4a) were segregated and partially embedded in the TiO_2 matrix (Figure 4b). This embedding is beneficial because it increases the contact surface between the two oxides, which is essential for charge transport. EDX mapping analysis confirms an increased homogeneity of the WO_3 distribution on the laser-treated surface compared to the untreated one (Figure 4e *vs.* Figure 4c). By processing the EDX maps, an increase of approximately 20% in the WO_3 coverage area (from 52.46% to 63.16%) is estimated (Figure 4f *vs.* Figure 4d). These improvements in distribution and the interface between the two oxides are considered to have a direct positive effect on the photoelectrocatalytic activity of the hybrid system

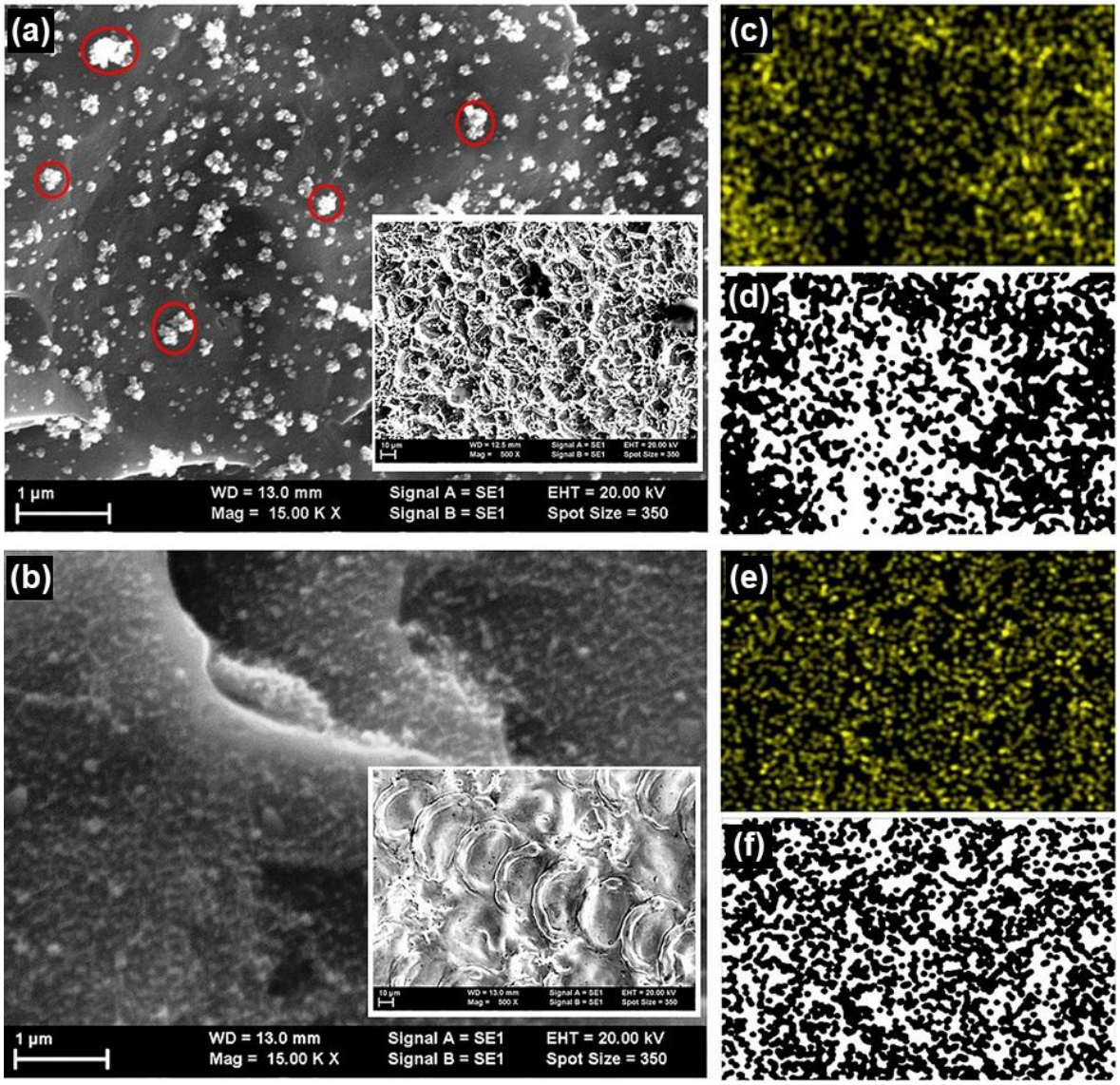

Figure 4. SEM images of the WO_3-decorated TiO_2 surface before (a) and after (b) the laser treatment. Insets: corresponding micrographs at lower magnification. Results of EDX mapping analysis for W-containing species at WO_3-TiO_2 (c) and L-WO_3-TiO_2 (e) together with their corresponding bitonal images (d and f, respectively).

X-ray Photoelectron Spectroscopy (XPS) confirmed the chemical modifications on the electrode surface induced by the laser treatment. The analysis of the W 4f spectra revealed a significant increase in the total relative W concentration (from 6.2% to 10.6%) at the surface of the L-WO_3-TiO_2 electrode, as a result of remodeling and improved dispersion of WO_3 particles, also observed by SEM-EDX. The most important finding is the increase in the relative quantity of the W^{5+} species (from 37% to 48% of the total W). The presence of W^{5+} is a direct indicator of oxygen vacancies at the surface [79,80], whose increased concentration contributes to the improvement of the photoelectrocatalytic activity.

Consistently, the O 1s spectra revealed a decrease in O^{2-} lattice species concentration (from 63.0% to 52.2%), confirming vacancy formation, along with an increase in adsorbed species (OH^- and H_2O), indicating more efficient adsorption on the laser-treated surface.

Photoelectrochemical measurements (LSV under UV illumination, Figure 5) show that the laser treatment increases the photocurrent by ~30% for the uncoated TiO_2 electrodes (L−TiO_2 *vs.* TiO_2, Figure 5), probably by increasing the surface area [73]. The WO_3 coating significantly improves performance due to enhanced light absorption (smaller band gap) and directed charge transfer at the WO_3-TiO_2 junction, which prevents recombination [81]. Additionally, oxygen vacancies (confirmed by XPS) contribute to efficient carrier separation by capturing and transferring the electrons [82]. The laser treatment applied to the WO_3-TiO_2 electrode (L-WO_3-TiO_2) further intensified the photoelectrocatalytic activity. Its effect is most pronounced at low potentials (below 0 V), where the oxygen evolution is strongly favored (inset Figure 5). At higher potentials, the effect decreases, the photocurrent ratio reaching a plateau of about 1.35 (above 0.45 V). Tafel measurements confirmed a significant shift in the oxygen evolution mechanism around 0 V, revealed by a sharp increase in the Tafel slope for both samples (*i.e.*, from 40 to 428 mV dec^{-1} for L-WO_3-TiO_2 and from 135 to 630 mV dec^{-1} for WO_3-TiO_2). Although the mechanism cannot be clearly identified, the laser treatment significantly accelerates the kinetics of oxygen evolution (three times lower Tafel slope below 0 V) by increasing the concentration of surface oxygen vacancies, which facilitates OH^- adsorption [83] and water split reaction [79].

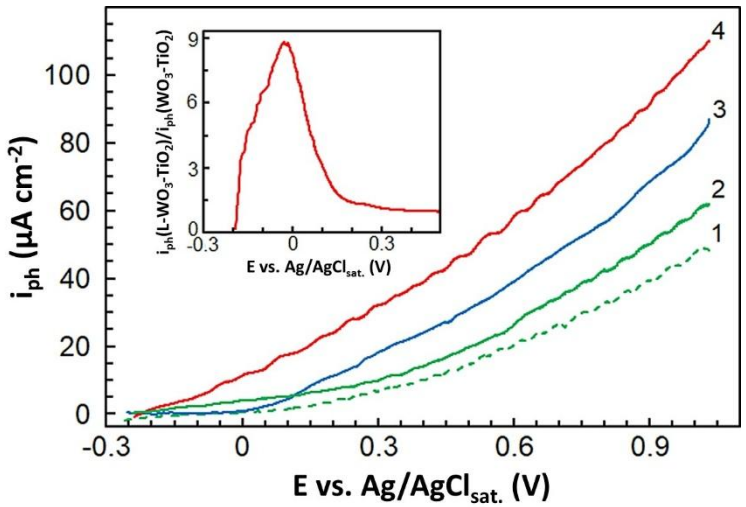

Figure 5. Linear sweep voltammograms (sweep rate, 10 mV s^{-1}) recorded under UV irradiation in 0.1 M KNO_3 + 0.01 M $HClO_4$ at pristine air-formed TiO_2 (1), laser-treated TiO_2 (2), untreated WO_3/TiO_2 (3) and laser-treated L-WO3-TiO_2 (4). Inset: effect of the potential on the photocurrents ratio for L-WO_3-TiO_2 and WO_3-TiO_2 electrodes.

Differential capacitance measurements (Mott-Schottky) confirmed the n-type semiconductor behavior for the hybrid electrodes. The laser treatment shifted the flat-band potential (E_{FB}) anodically by ~130mV (from −0.359V to −0.231V) for the L-WO_3-TiO_2 sample. Furthermore, assuming that the laser treatment does not significantly modify the dielectric constant, a ~10% increase in the donor concentration (N_D) was estimated for L−WO_3-TiO_2, which contributes to the increase in photocurrent. Although the anodic shift of E_{FB} is theoretically unfavorable, the much more efficient charge carrier separation in the laser-treated electrode compensates for this effect, resulting in a superior photocurrent [84].

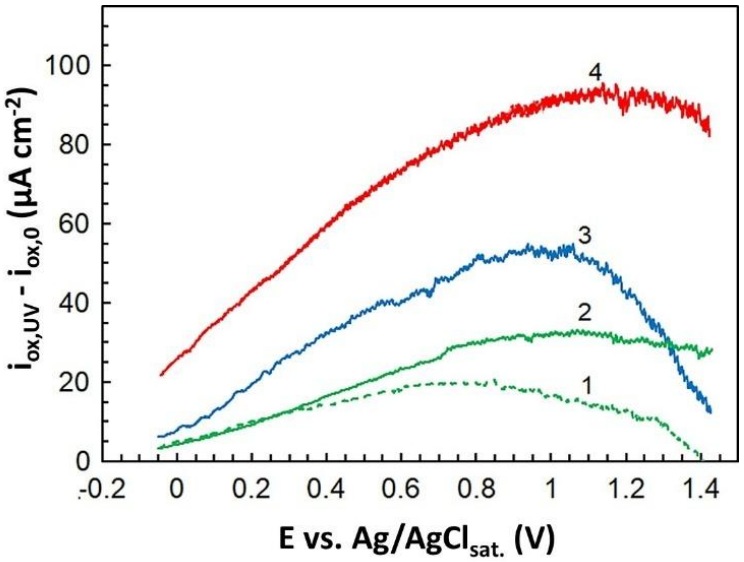

Figure 6. Influence of the applied potential on the difference between the methanol oxidation current under UV ($i_{ox,UV}$) and its corresponding value observed in dark ($i_{ox,0}$) for pristine TiO_2 (1), laser-treated TiO_2 (2), WO_3/TiO_2 (3) and L-WO_3/TiO_2 (4). Electrolyte solution: 0.5 M H_2SO_4 + 2.25 M CH_3OH.

Both tungsten oxide (WO_3) and WO_3-TiO_2 hybrids have been proposed as suitable photoanodes for photoelectrochemical degradation of a wide variety of organic water pollutants [85,86]. The use of laser treatment to improve the photoelectrocatalytic properties of WO_3-coated TiO_2 electrodes was evaluated through the photoelectrochemical oxidation reaction of methanol. Linear Sweep Voltammetry (LSV) measurements were performed under UV irradiation and in the dark, with the photoassisted oxidation current ($i_{ox,UV}$-$i_{ox,0}$) being represented in Figure 6. In the case of uncoated TiO_2 electrodes, the laser treatment had a minor effect, with improvement visible only at potentials higher than 0.3 V, suggesting an increase in charge carrier separation efficiency. The untreated WO_3-TiO_2 electrode (curve 3) shows an increase in methanol oxidation under UV up to ~0.8 V, after which it decreases,

indicating that at high anodic potentials, the process is controlled by the external source. In contrast, the laser-treated electrode (L-WO_3-TiO_2, curve 4) shows a much more significant influence of UV light. The pronounced improvement in photoanodic activity cannot be explained solely by the approximately 10% increase in donor concentration, primarily being attributed to the much greater efficiency of charge carrier separation, induced by the laser treatment. An essential secondary factor is the high concentration of OH^- species (XPS), which contributes to increased efficiency by facilitating the desorption of oxidation products and maintaining the activity of the catalytic centers [87].

3.3. Enhancement of the capacitive features of WO_3 supported on pristine and functionalized graphite by appropriate adjustment of the electrodeposition regime [76]

3.3.1. Introduction

To meet current energy demands, supercapacitors are increasingly employed as storage systems, owing to their high power density and fast charge–discharge rates [88,89]. They are classified as electrochemical double-layer capacitors (EDLCs), which store energy electrostatically, and pseudocapacitors, which store energy chemically via fast and reversible faradaic reactions, thereby achieving higher capacities [89,90]. In this context, transition metal oxides, such as ZnO, VO_2, and MnO_2, are extensively studied as advanced electrode materials and incorporated into various composites [91–93]. A highly promising approach for developing high-performance supercapacitors involves the use of tungsten trioxide (WO_3) as electrode material, owing to its structural stability and good conductivity [94], as well as its ability to accommodate structural transformations and substoichiometric phase transitions [95].

To obtain WO_3-based supercapacitor electrodes with enhanced capacity, efficient platforms are required. In this regard, carbon nanomaterials (*e.g.*, graphene, CNTs) are considered excellent substrates due to their low cost, large specific surface area, and high electrical conductivity [96,97]. These form synergistic composites, such as WO_3-rGO (reduced graphene oxide) on carbon paper, improving capacitive performance [88,98,99]. In addition to the substrate, the synthesis method of WO_3 is crucial. Among various techniques (*e.g.*, sputtering [100], hydrothermal synthesis [101,102], CVD [103] *etc.*), electrodeposition

stands out due to its low cost and control over the deposited layer [104,105]. The morphology and particle size of WO_3 (*e.g.*, smaller with pulsed electrodeposition) vary significantly with the electrodeposition regime, directly affecting the capacitive properties [106,107].

Based on the aspects mentioned above, this work investigates the effect of the WO_3 electrodeposition method (pulsed and continuous regime) on its capacitive behavior when deposited onto a graphite (G) substrate. To enhance performance, the study is further extended to WO_3 deposited on graphite substrates modified by functionalization with reduced Graphene Oxide (rGO) or Carbon Nanowalls (CNW). In addition, detailed investigations of the structure and surface chemistry are carried out. The main objective of this research is to obtain electrode materials with superior capacitive performance, while also aiming to provide a better understanding of key factors that influence the behavior of these hybrid systems.

3.3.2. Materials and methods

3.3.2.1. Preparation of CNW/G and rGO/G

To obtain performant supercapacitor electrodes, graphite (G) substrates were modified with rGO or CNW. The rGO films were applied using the drop-cast method, following a plasma pre-treatment of the graphite to increase its hydrophilic character and ensure uniform distribution of the suspension [108]. On the other hand, the CNW layer was grown using the RFPECVD (Radio Frequency Plasma-Enhanced Chemical Vapor Deposition) technique, employing an $Ar/H_2/C_2H_2$ mixture and maintaining the substrate at 700 °C. The 50-minute process resulted in films approximately 2 μm thick [109–111].

3.3.2.2. Deposition and electrochemical characterization of WO_3 on bare and modified graphite

The substrates modification with WO_3 was achieved by electrodeposition from an aqueous solution of Na_2WO_4 in the presence of $HClO_4$ and H_2O_2 [107]. Two techniques were employed, both at a potential of -0.7 V: continuous electrodeposition (CE) and pulsed electrodeposition (PE) (0.5 s pulses followed by a 1.5 s open-circuit rest). The substrates included graphite (G) plates, which were either pristine (native) (WO_3/G), or functionalized with rGO (WO_3/rGO/G) or CNW (WO_3/CNW/G). The resulting notations reflect the method (*e.g.*, WO_3/G for CE and WO_3/G-PE for PE on pristine graphite), allowing for a comparative evaluation of the influence of the deposition regime and substrate functionalization.

3.3.3. Results and discussion

Cyclic voltammetry (CV) measurements, performed to evaluate the electrochemical properties and stability of WO_3/G (continuous deposition) and WO_3/G-PE (pulsed deposition) electrodes in 0.5 M H_2SO_4, revealed that both materials exhibit a similar voltammetric profile, indicating the presence of two redox couples. These couples, absent on the bare graphite electrode, demonstrate that the observed phenomena arise from electron transfer within the WO_3 layer, associated with the intercalation/deintercalation and insertion/de-insertion processes of hydrated H^+ ions into the oxide structure [106,107,112]. The specific capacitance evaluation, calculated by integrating the voltammograms, revealed a considerable increase following the modification with WO_3: from 0.16 mF cm^{-2} for the bare graphite, to 8.5 mF cm^{-2} for WO_3/G and 1.25 mF cm^{-2} for WO_3/G-PE. These results highlight that the electrode obtained by continuous regime deposition (WO_3/G) exhibits markedly superior capacitive performance, having the specific capacitance seven times higher than that of the pulsed regime electrode. Despite the inability to calculate gravimetric capacitance precisely, the superiority of the continuous approach is evident.

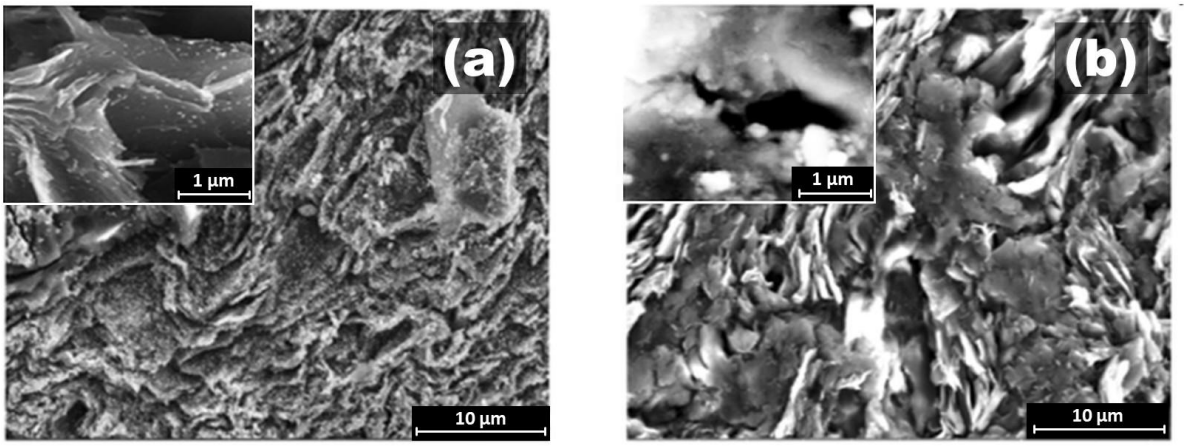

Figure 7. SEM micrographs of WO_3/G-PE (a), and WO_3/G (b) electrodes surfaces.

Surface morphology analysis via SEM was crucial to understand the difference in capacitive performance between the electrodes (Figure 7). In the case of pulsed electrodeposition (WO_3/G-PE), alternating the deposition potential with the rest potential (open circuit) allowed for the removal of the diffusion layer, resulting in uniform, small-sized WO_3 nanoparticles. In contrast, by interruptingly applying the potential for continuous electrodeposition (WO_3/G), preferential nucleation occurred on the more conductive regions of the graphite, resulting in the formation of large conglomerates and a non-uniform

distribution. Although the morphology obtained by the pulsed method is considered optimal (uniform nanoparticles), the superior specific capacitance of the WO_3/G electrode suggests that the dominant factor was the larger mass of WO_3 deposited in the continuous regime, which compensated for the non-uniformity. Despite the fact that the uniform distribution of WO_3 nanoparticles obtained by pulsed deposition (WO_3/G-PE) should result in a greater number of active sites, the superior capacitive results of the continuously deposited electrode (WO_3/G) suggest that the larger mass (quantity) of deposited oxide, indicated by the formation of larger conglomerates observed in SEM, is the dominant factor explaining the performance improvement. This conclusion is supported by the XPS survey analysis, which shows a relatively higher W concentration on the surface of WO_3/G (0.8%) compared to WO_3/G-PE (0.5%), in line with the morphological observations.

High-resolution XPS analysis (W 4f) revealed the chemical surface differences between the electrodes. The surface of the WO_3/G-PE sample (pulsed regime), contains only W^{6+} species (WO_3), indicating the formation of an undoped oxide [107,113–116]. In contrast, the WO_3/G sample (continuous regime) revealed the major presence of W^{6+} (90.3%), but also a small amount of lower valence W (9.7%), attributed to W^{5+} [112, 113]. The presence of W^{5+} suggests that, during continuous cathodic deposition, H^+ ions are inserted into the WO_3 lattice, dilating it and significantly increasing the electrical conductivity [113,117,118]. These findings indicate that the continuous deposition method (WO_3/G) outperforms the pulsed approach, providing higher oxide loading and facilitating H^+ intercalation into the lattice (formation of W^{5+}). This leads to a less rigid WO_3 structure and superior electrical conductivity, which is directly responsible for the enhanced capacitive performance of the electrode.

Although the WO_3/G electrodes exhibit good capacitive properties, performance can be significantly improved by using graphite substrates functionalized with rGO or CNW, both materials being recognized for their large specific surface area and excellent conductivity [97,119,120].

The cyclic voltammograms of the WO_3/CNW/G and WO_3/rGO/G electrodes reveal significant faradaic differences (Figure 8). The WO_3/CNW/G electrode exhibits two clear redox couples, confirming the occurrence of both intercalation/deintercalation processes of hydrated H^+ ions (from surface/pores, I, and from the bulk solution, II) [106,107,121]. In contrast, for the WO_3/rGO/G electrode, the intercalation of H^+ ions from the bulk solution

(II) is not clearly visible. These observations and the quasi-rectangular shape suggest that the charge storage mechanism of these electrodes originates from both ion accumulation in the electrochemical double layer and redox (pseudocapacitive) processes [89,90,122,123].

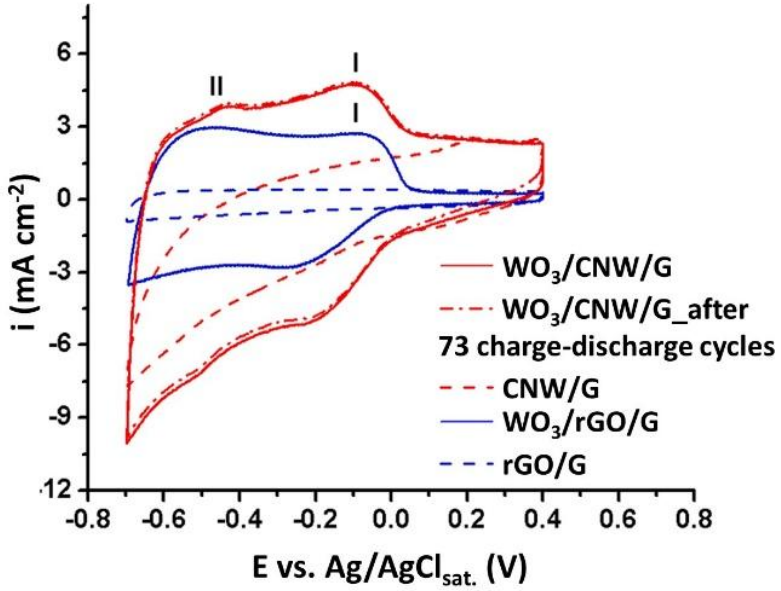

Figure 8. Cyclic voltammograms of WO_3/CNW/G (solid red curve), WO_3/CNW/G (dash-dot red curve) after charge–discharge 73 cycles, CNW/G (dashed red curve), WO_3/rGO/G (solid blue curve) and rGO/G (dashed blue curve) at 50 mV s^{-1} in 0.5 M H_2SO_4.

Specific capacitance estimated from the cyclic voltammograms indicates that the WO_3/CNW/G electrode reaches a value of ~78 mF cm^{-2}, nearly 9 times higher than WO_3/G. At the same time, the WO_3/rGO/G electrode registers a capacitance of ~35 mF cm^{-2}, about 4 times higher than WO_3/G, highlighting that rGO and CNW significantly enhance capacitive performance by modifying the surface chemistry and morphology.

Cyclic voltammograms at different scan rates showed that the WO_3/CNW/G electrode retains its quasi-rectangular shape even at high rates, unlike WO_3/rGO/G, where the voltammograms become distorted, indicating lower internal resistance and superior capacitive performance for the CNW-modified electrode. Charge density estimations confirmed that WO_3/CNW/G consistently stores more charge than WO_3/rGO/G (188 mC cm^{-2} *vs.* 104 mC cm^{-2}). These results demonstrate that the use of the CNW-modified substrate increases the accessibility of WO_3 to the electrolyte, promoting redox processes and ion adsorption, which leads to a significantly enhanced storage capacity.

Morphology (SEM) and composition (EDX) analysis justifies the superior performance of the CNW/G substrate (Figure 9). It exhibits interconnected graphene nanowalls, oriented perpendicularly to the graphite, an architecture beneficial for charge transport and one that offers a large apparent surface area with excellent electrolyte accessibility [91]. The deposition of WO_3 on this substrate does not dramatically change the morphology (Figure 9c *vs.* Figure 9a) and is uniformly distributed (EDX), creating a synergistic effect that explains the remarkable capacitive performances of the WO_3/CNW/G electrode. In contrast, rGO/G forms a non-homogeneous layer of graphene sheets (Figure 9b), leading to increased internal resistance and a smaller apparent surface area due to random distribution. The deposition of WO_3 over rGO/G forms a compact, cracked film (Figure 9d) that does not enhance the surface area exposed to the electrolyte, resulting in lower capacity and increased electrical resistance, consistent with CV results. Thus, functionalizing the graphite substrate with CNW ensures a better WO_3 distribution and a larger apparent surface area, significantly improving the capacitive properties.

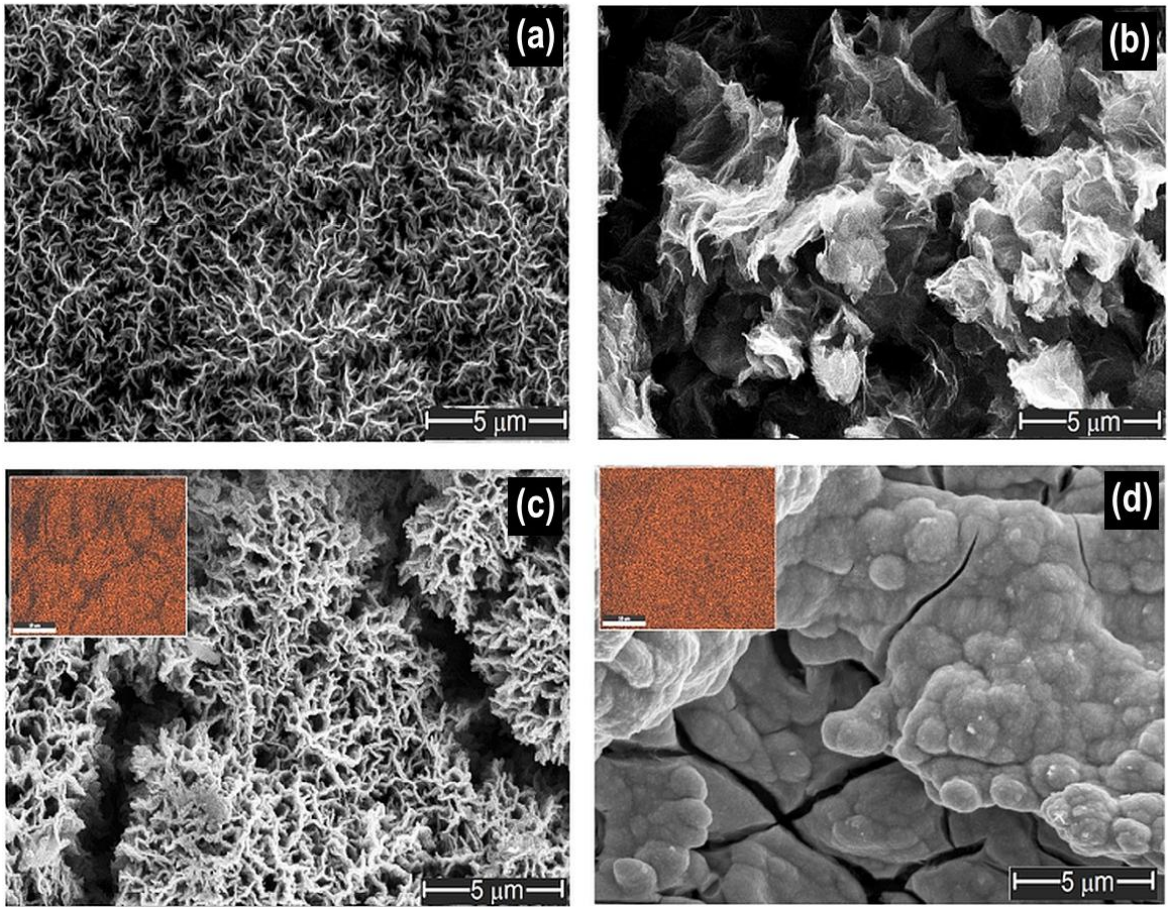

Figure 9. SEM micrographs of CNW/G (a), rGO/G (b), WO_3/CNW/G (c) and WO_3/rGO/G (d); Insets: Mapping EDX analysis of WO_3/CNW/G (c) and WO/rGO/G (d).

XPS analysis (W 4f) confirmed that all electrodes obtained by continuous electrodeposition regime (WO_3/G, WO_3/CNW/G, and WO_3/rGO/G) contain both oxidation states, W^{6+} and W^{5+}, in a ratio of ~9/1. This indicates that H^+ ion insertion into the WO_3 lattice is determined not by the nature of the carbonaceous substrate, but by the electrodeposition regime. Moreover, the C 1s analysis provides insight into the degree of disorder within the carbon matrix, which can partially account for the electrode performance. Thus, the ~1.8-fold higher percentage of Csp^3 species for the WO_3/rGO/G electrode compared to WO_3/CNW/G (27.3% *vs.* 14.7%) indicates a higher degree of disorder, which can reduce the electrical conductivity of the material [124,125]. Furthermore, WO_3/rGO/G has a higher amount of oxygenated carbon species (28.8% *vs.* 20.7%), which can block the surface and hinder electron transfer and H^+ insertion, thereby reducing the pseudocapacitive component and, implicitly, the total capacity.

Galvanostatic charge-discharge measurements (2 mA cm^{-2}) confirmed the superior performance of the WO_3/CNW/G electrode. The results revealed a predominantly electrostatic charge storage mechanism, reflected by the nearly linear charge–discharge profiles. Nevertheless, a noticeable deviation from linearity for the WO_3/CNW/G electrode confirms the pseudocapacitive contribution observed in cyclic voltammetry [126,127]. The specific capacitance calculated from the charge-discharge measurements was 66.3 mF cm^{-2} for WO_3/CNW/G and 50.5 mF cm^{-2} for WO_3/rGO/G. The improved performance of WO_3/CNW/G is due to the interconnected WO_3-CNW-graphite structure, which ensures a large accessible surface area, low internal resistance, and a significant pseudocapacitive contribution, favored by the continuous electrodeposition regime. Furthermore, the WO_3/CNW/G electrodes display good stability, with only ~6% capacity loss after 73 charge-discharge cycles (Figure 8).

4. CONCLUSIONS AND PERSONAL CONTRIBUTIONS

The urgent need for sustainable solutions to the global energy crisis directed this work towards the **development of advanced electrode materials** for the conversion and **storage of renewable energy**. The approach focused on **optimizing electrochemical systems**,

concentrating on increasing the efficiency of water electrolysis and developing high-performance electrodes for supercapacitors:

1. Optimization of the Oxygen Evolution Reaction (OER)

- An **innovative method** was developed to obtain high-performance Co-Ni anodes through **thermal interpenetration of metals** followed by calcination.
- The resulting electrodes demonstrated **superior electrocatalytic activity** (the lowest Tafel slopes and minimum reaction onset potential) and **good stability**.
- The efficiency is primarily due to remarkable **oxidation resistance**, **low electrical resistance** of the active phase film, and **increased surface hydrophilicity**.

2. Improvement of WO_3−TiO_2 photoanodes

- The **beneficial role of WO_3-TiO_2 junctions** in enhancing the efficiency of **photoelectrochemical anodic oxidation processes** was confirmed.
- Applying a **laser treatment** to the WO_3−TiO_2 electrodes with optimal composition **significantly improved** their **performance**, evidenced by superior photocurrents and a minimum onset potential.
- The improvement was attributed to the **uniform segregation of WO_3**, the **increase in oxygen vacancies**, **better separation of photogenerated charge carriers**, and the **higher donor concentration**, resulting in **enhanced efficiency** in photo-assisted oxidation processes of water and methanol.

3. Development of Supercapacitor Electrodes

- It was established that **continuous regime electrodeposition of WO_3** is **superior** to pulsed deposition, due to obtaining a **larger quantity of oxide** and the **intercalation of H^+ ions** into the oxide lattice, which improves electrical conductivity and pseudocapacitive contribution.
- The use of **functionalized** graphite substrates significantly increased performance: the specific capacitance of WO_3/CNW/G was approximately **nine times higher** (and four times higher for WO_3/rGO/G) compared to the pristine substrate.

- The exceptional performance of the **WO_3/CNW/G** electrode originates from the **interconnected WO_3-CNW-grafit structure**, which ensures **high electrical conductivity**, **high double-layer capacity** (large surface area exposed to the electrolyte), and a **superior faradaic contribution**.

Therefore, these studies make important contributions to the field of electrode materials, offering high-performance and sustainable solutions for renewable energy conversion and storage systems.

5. PUBLICATIONS AND DISSEMINATION

5.1. Publications included in the thesis

1. **Mihai MA**, Preda L, Negrila C, Somacescu S, Becherescu ND, Velea A, Zaki MY, Spataru N. Thermally Interpenetrated Co–Ni Mixed Oxide as Efficient Oxygen Evolution Electrodes. Electrocatalysis. 2025 July;16(4):758–71.. **IF: 2,8** https://doi.org/10.1007/s12678-025-00956-4

2. Spătaru T, **Mihai MA**, Preda L, Marcu M, Radu MM, Becherescu ND, Velea A, Zaki MY, Udrea R, Satulu V, Spătaru N. Enhanced photoelectrochemical activity of WO3-decorated native titania films by mild laser treatment. Applied Surface Science. 2022;596:153682. **IF: 7,4** https://doi.org/10.1016/j.apsusc.2022.153682

3. Marcu M, Preda L, Vizireanu S, Bita B, **Mihai MA**, Spataru T, Acsente T, Dinescu G, Spataru N. Enhancement of the capacitive features of WO3 supported on pristine and functionalized graphite by appropriate adjustment of the electrodeposition regime. Materials Science and Engineering: B. 2022 Mar;277:115585. **IF: 3,4** https://doi.org/10.1016/j.mseb.2021.115585

6. REFERENCES

1. Al-Ghussain L. Global warming: review on driving forces and mitigation. Environmental Progress & Sustainable Energy. 2019 Jan 1;38(1):13–21.

2. McKay DIA, Staal A, Abrams JF, Winkelmann R, Sakschewski B, Loriani S, et al. Exceeding 1.5°C global warming could trigger multiple climate tipping points. Science. 2022;377(6611):eabn7950.

3. Riebeek H. Global Warming [Internet]. NASA. Available from: https://earthobservatory.nasa.gov/features/GlobalWarming

4. United Nations Framework Convention on Climate Change. The Paris Agreement [Internet]. Available from: https://unfccc.int/process-and-meetings/the-paris-agreement

5. IEA (2021). Net Zero by 2050. IEA [Internet]. 2021; Available from: https://www.iea.org/reports/net-zero-by-2050, License: CC BY 4.0

6. Ritchie H, Rosado P. Fossil fuels. Our World in Data [Internet]. 2017; Available from: https://ourworldindata.org/fossil-fuels

7. Zhang Z, Ding T, Zhou Q, Sun Y, Qu M, Zeng Z, et al. A review of technologies and applications on versatile energy storage systems. Renewable and Sustainable Energy Reviews. 2021;148:111263.

8. Ishaq H, Dincer I, Crawford C. A review on hydrogen production and utilization: Challenges and opportunities. International Journal of Hydrogen Energy. 2022;47(62):26238–64.

9. Aminudin MA, Kamarudin SK, Lim BH, Majilan EH, Masdar MS, Shaari N. An overview: Current progress on hydrogen fuel cell vehicles. International Journal of Hydrogen Energy. 2023;48(11):4371–88.

10. Mahajan D, Tan K, Venkatesh T, Kileti P, Clayton CR. Hydrogen Blending in Gas Pipeline Networks—A Review. Energies. 2022 May 13;15(10):3582.

11. Franco A, Giovannini C. Recent and Future Advances in Water Electrolysis for Green Hydrogen Generation: Critical Analysis and Perspectives. Sustainability. 2023;15(24).

12. Stefanizzi M, Capurso T, Filomeno G, Torresi M, Pascazio G. Recent Combustion Strategies in Gas Turbines for Propulsion and Power Generation toward a Zero-Emissions Future: Fuels, Burners, and Combustion Techniques. Energies [Internet]. 2021;14(20). Available from: https://www.mdpi.com/1996-1073/14/20/6694

13. Capurso T, Stefanizzi M, Torresi M, Camporeale SM. Perspective of the role of hydrogen in the 21st century energy transition. Energy Conversion and Management. 2022;251:114898.

14. Millet P, Grigoriev S. Chapter 2 - Water Electrolysis Technologies. In: Gandía LM, Arzamendi G, Diéguez PM, editors. Renewable Hydrogen Technologies [Internet]. Amsterdam: Elsevier; 2013. p. 19–41. Available from: https://www.sciencedirect.com/science/article/pii/B9780444563521000027

15. Dong G, Yan L, Bi Y. Advanced oxygen evolution reaction catalysts for solar-driven photoelectrochemical water splitting. J Mater Chem A. 2023;11(8):3888–903.

16. Lin YC, Wyżga P, Macyk J, Macyk W, Guzik MN. Solar-driven (photo)electrochemical devices for green hydrogen production and storage: Working principles and design. Journal of Energy Storage. 2024 Mar 30;82:110484.

17. Exeler J, Jüstel T. Advances in Functional Ceramics for Water Splitting: A Comprehensive Review. Photochem. 2024;4(2):271–84.

18. Chatenet M, Pollet BG, Dekel DR, Dionigi F, Deseure J, Millet P, et al. Water electrolysis: from textbook knowledge to the latest scientific strategies and industrial developments. Chem Soc Rev. 2022;51(11):4583–762.

19. Yanzhao Zhang, Dazhi Yao, Jinzhe Liu, Zhiliang Wang, Lianzhou Wang. Advancing strategies on green H2 production via water electrocatalysis: bridging the benchtop research with industrial scale-up. Microstructures. 2024;4(2):2024020.

20. Shih AJ, Monteiro MCO, Dattila F, Pavesi D, Philips M, da Silva AHM, et al. Water electrolysis. Nature Reviews Methods Primers. 2022 Oct 27;2(1):84.

21. Mihai MA, Preda L, Negrila C, Somacescu S, Becherescu ND, Velea A, et al. Thermally Interpenetrated Co–Ni Mixed Oxide as Efficient Oxygen Evolution Electrodes. Electrocatalysis. 2025 July;16(4):758–71.

22. Han N, Zhang W, Guo W, Pan H, Jiang B, Xing L, et al. Designing Oxide Catalysts for Oxygen Electrocatalysis: Insights from Mechanism to Application. Nano-Micro Lett. 2023 Dec;15(1):185.

23. Han N, Zhang X, Zhang C, Feng S, Zhang W, Guo W, et al. Lowering the kinetic barrier via enhancing electrophilicity of surface oxygen to boost acidic oxygen evolution reaction. Matter. 2024 Mar;7(3):1330–43.

24. Fabbri E, Habereder A, Waltar K, Kötz R, Schmidt TJ. Developments and perspectives of oxide-based catalysts for the oxygen evolution reaction. Catal Sci Technol. 2014;4(11):3800–21.

25. Cherevko S, Geiger S, Kasian O, Kulyk N, Grote JP, Savan A, et al. Oxygen and hydrogen evolution reactions on Ru, RuO2, Ir, and IrO2 thin film electrodes in acidic and alkaline electrolytes: A comparative study on activity and stability. Catalysis Today. 2016 Mar 15;262:170–80.

26. Huo X, Yu H, Xing B, Zuo X, Zhang N. Review of High Entropy Alloys Electrocatalysts for Hydrogen Evolution, Oxygen Evolution, and Oxygen Reduction Reaction. The Chemical Record. 2022 Dec;22(12):e202200175.

27. Wang H, Zhu S, Deng J, Zhang W, Feng Y, Ma J. Transition metal carbides in electrocatalytic oxygen evolution reaction. Chinese Chemical Letters. 2021 Jan;32(1):291–8.

28. Zubair M, Ul Hassan MM, Mehran MT, Baig MM, Hussain S, Shahzad F. 2D MXenes and their heterostructures for HER, OER and overall water splitting: A review. International Journal of Hydrogen Energy. 2022 Jan;47(5):2794–818.

29. Kim JS, Kim B, Kim H, Kang K. Recent Progress on Multimetal Oxide Catalysts for the Oxygen Evolution Reaction. Advanced Energy Materials. 2018 Apr;8(11):1702774.

30. Yu M, Budiyanto E, Tüysüz H. Principles of Water Electrolysis and Recent Progress in Cobalt-, Nickel-, and Iron-Based Oxides for the Oxygen Evolution Reaction. Angew Chem Int Ed. 2022 Jan 3;61(1):e202103824.

31. Song F, Bai L, Moysiadou A, Lee S, Hu C, Liardet L, et al. Transition Metal Oxides as Electrocatalysts for the Oxygen Evolution Reaction in Alkaline Solutions: An Application-Inspired Renaissance. J Am Chem Soc. 2018 June 27;140(25):7748–59.

32. Yu N, Ma Y, Ren JK, Zhang ZJ, Liu HJ, Nan J, et al. High negative voltage activating perovskite oxide with bi-vacancy synergistic regulation for water oxidation. Chemical Engineering Journal. 2023 Dec;478:147415.

33. Burke MS, Enman LJ, Batchellor AS, Zou S, Boettcher SW. Oxygen Evolution Reaction Electrocatalysis on Transition Metal Oxides and (Oxy)hydroxides: Activity Trends and Design Principles. Chem Mater. 2015 Nov 24;27(22):7549–58.

34. Subbaraman R, Tripkovic D, Chang KC, Strmcnik D, Paulikas AP, Hirunsit P, et al. Trends in activity for the water electrolyser reactions on 3d M(Ni,Co,Fe,Mn) hydr(oxy)oxide catalysts. Nature Mater. 2012 June;11(6):550–7.

35. Han N, Race M, Zhang W, Marotta R, Zhang C, Bokhari A, et al. Perovskite and related oxide based electrodes for water splitting. Journal of Cleaner Production. 2021 Oct;318:128544.

36. Badruzzaman A, Yuda A, Ashok A, Kumar A. Recent advances in cobalt based heterogeneous catalysts for oxygen evolution reaction. Inorganica Chimica Acta. 2020 Oct;511:119854.

37. Chen Y, Rui K, Zhu J, Dou SX, Sun W. Recent Progress on Nickel-Based Oxide/(Oxy)Hydroxide Electrocatalysts for the Oxygen Evolution Reaction. Chemistry A European J. 2019 Jan 14;25(3):703–13.

38. Filimonenkov IS, Bouillet C, Kéranguéven G, Simonov PA, Tsirlina GA, Savinova ER. Carbon materials as additives to the OER catalysts: RRDE study of carbon corrosion at high anodic potentials. Electrochimica Acta. 2019 Oct;321:134657.

39. Haynes WM, editor. CRC Handbook of Chemistry and Physics. In: 97th ed. CRC Press; 2016 [cited 2025 Aug 25]. p. 14–7. Available from: https://www.taylorfrancis.com/books/9781498754293

40. Knözinger H, Taglauer E. Spreading and Wetting. In: Ertl G, Knözinger H, Weitkamp J, editors. Preparation of Solid Catalysts [Internet]. 1st ed. Wiley; 1999 [cited 2025 Aug 25]. p. 501–26. Available from: https://onlinelibrary.wiley.com/doi/10.1002/9783527619528.ch4h

41. Million B, Kučera J. Concentration dependence of diffusion of cobalt in nickel-cobalt alloys. Acta Metallurgica. 1969 Mar;17(3):339–44.

42. Chi B, Lin H, Li J, Wang N, Yang J. Comparison of three preparation methods of NiCo2O4NiCo2O4 electrodes. International Journal of Hydrogen Energy. 2006 Aug;31(9):1210–4.

43. Chi B. Effect of temperature on the preparation and electrocatalytic properties of a spinel NiCo2O4/Ni electrode. International Journal of Hydrogen Energy. 2004 May;29(6):605–10.

44. Li G, Anderson L, Chen Y, Pan M, Abel Chuang PY. New insights into evaluating catalyst activity and stability for oxygen evolution reactions in alkaline media. Sustainable Energy Fuels. 2018;2(1):237–51.

45. Kuboon S, Hu YH. Study of NiO−CoO and Co_3O_4 −Ni_3O_4 Solid Solutions in Multiphase Ni−Co−O Systems. Ind Eng Chem Res. 2011 Feb 16;50(4):2015–20.

46. Roginskaya YuE, Morozova OV, Lubnin EN, Ulitina YuE, Lopukhova GV, Trasatti S. Characterization of Bulk and Surface Composition of $Co_x Ni_{1-x} O_y$ Mixed Oxides for Electrocatalysis. Langmuir. 1997 Aug 1;13(17):4621–7.

47. Bajdich M, García-Mota M, Vojvodic A, Nørskov JK, Bell AT. Theoretical Investigation of the Activity of Cobalt Oxides for the Electrochemical Oxidation of Water. J Am Chem Soc. 2013 Sept 11;135(36):13521–30.

48. Wang HY, Hung SF, Chen HY, Chan TS, Chen HM, Liu B. In Operando Identification of Geometrical-Site-Dependent Water Oxidation Activity of Spinel Co_3O_4. J Am Chem Soc. 2016 Jan 13;138(1):36–9.

49. Mondal R, Ratnawat H, Kumar S, Kumar A, Singh P. Ni stabilized rock-salt structured CoO; $Co_{1-x} Ni_x O$: tuning of e_g electrons to develop a novel OER catalyst. RSC Adv. 2020;10(30):17845–53.

50. Jin Y, Li Z, Wang J, Li R, Li Z, Liu H, et al. Tuning Spin State of Rock-Salt-Based Oxides by Manipulation of Crystallinity for Efficient Oxygen Electrocatalysis. Advanced Energy Materials. 2018 Aug;8(22):1703469.

51. He Y, Han XP, Rao DW, Zhang YD, Zhao J, Zhong C, et al. Charge redistribution of Co on cobalt (II) oxide surface for enhanced oxygen evolution electrocatalysis. Nano Energy. 2019 July;61:267–74.

52. Jin Z, Bard AJ. Atom-by-atom electrodeposition of single isolated cobalt oxide molecules and clusters for studying the oxygen evolution reaction. Proc Natl Acad Sci USA. 2020 June 9;117(23):12651–6.

53. Spătaru T, Mihai MA, Preda L, Marcu M, Radu MM, Becherescu ND, et al. Enhanced photoelectrochemical activity of WO3-decorated native titania films by mild laser treatment. Applied Surface Science. 2022;596:153682.

54. Fujishima A, Honda K. Electrochemical photolysis of water at a semiconductor electrode. Nature. 1972;238(5358):37–8.

55. Hashimoto K, Irie H, Fujishima A. TiO2 photocatalysis: A historical overview and future prospects. Jpn J Appl Phys. 2005;44(12):8269–85.

56. Bakbolat B, Daulbayev C, Sultanov F, Beissenov R, Umirzakov A, Mereke A, et al. Recent developments of TiO2-based photocatalysis in the hydrogen evolution and photodegradation: A review. Nanomaterials. 2020;10(9).

57. Chen X, Mao SS. Titanium dioxide nanomaterials: synthesis, properties, modifications, and applications. Chem Rev. 2007;107:2891–959.

58. Serpone N. Is the band gap of pristine TiO2 narrowed by anion and cation doping of titanium dioxide of second-generation photocatalysts? J Phys Chem B. 2006;110:24287–93.

59. Padmanabhan SC, Pillai SC, Colreavy J, Balakrishna J, McCormak DE, Perova TS, et al. A simple sol-gel processing for the development of high temperature stable photoactive anatase titania. Chem Mater. 2007;19:4474–81.

60. Irie H, Watanabe Y, Hashimoto K. Carbon doped anatase TiO2 powders as visible light sensitive photocatalyst. Chem Lett. 2003;32:772–3.

61. Sakthivel S, Kisch H. Daylight photocatalysis by carbon-modified titanium dioxide, Angew. Chem Int Ed. 2003;42(40):4908–11.

62. Umebayashi T, Yamaki T, Itoh H, Asai K. Band gap narrowing of titanium dioxide by sulfur doping. Appl Phys Lett. 2002;81(3):454–6.

63. Likodimos V, Stergiopoulos T, Falaras P, Kuntze J, Schmuki P. Phase composition, size, orientation and antenna effects on self-assembled anodized titania nanotube arrays. A polarized micro-Raman investigation. J Phys Chem C. 2008;112:12687–96.

64. Chen X, Liu L, Yu PY, Mao SS. Increasing solar absorption for photocatalysis with black hydrogenated titanium dioxide monocrystals. Science. 2011;331:746–50.

65. Dozzi MV, Prati L, Canton P, Selli E. Effects of gold nanoparticles deposition on the photocatalytic activity of titanium dioxide under visible light. Phys Chem Chem Phys. 2009;11(33):7171.

66. Dozzi MV, Saccomanni A, Altomare M, Selli E. Photocatalytic activity of NH4F-doped TiO2 modified by noble metal nanoparticle deposition. Photochem Photobiol Sci. 2013;12(4):595–601.

67. Mashtalir O, Kurtoglu M, Pogulay S, Gogotsi A, Naguib M, Gogotsi Y. Photocatalytic WO3 and TiO2 films on brass. Int J Appl Ceram Tech. 2013;10(1):26–32.

68. Linsebigler AL, Lu G, Yates JT Jr. Photocatalysis on TiO2 surfaces: principles, mechanisms, and selected results. Chem Rev. 1995;95:735–58.

69. Paramasivam I, Nah YC, Das C, Shrestha N, Schmuki P. WO3/TiO2 nanotubes with strongly enhanced photocatalytic activity. Chem Eur J. 2010;16(30):8993–7.

70. Anandan S, Sivasankar T, Lana-Villarreal T. Synthesis of TiO2/WO3 nanoparticles via sonochemical approach for the photocatalytic degradation of methylene blue under visible light illumination, Ultrason. Sonochem. 2014;21(6):1964–8.

71. Luo X, Deng F, Min L, Luo S, Guo B, Zeng G, et al. Facile one-step synthesis of inorganic-framework molecularly imprinted TiO2/WO3 nanocomposite and its molecular recognitive photocatalytic degradation of target contaminant, Environ. Sci Technol. 2013;47(13):7404–12.

72. Nakata K, Kagawa T, Sakai M, Liu S, Ochiai T, Sakai H, et al. Preparation and photocatalytic activity of robust titania monoliths for water remediation. ACS Appl Mater Interfaces. 2013;5(3):500–4.

73. Radu MM, Becherescu N, Spataru T, Osiceanu P, Mihai MA, Calderon-Moreno JM, et al. Improved suitability as catalyst support and more efficient charge carrier separation of native air-formed TiO2 films by mild laser treatment. J Power Sources. 2019;437:226921.

74. Battisti AD, Lodi G, Cappadonia M, Battaglin G, Kotz R. Influence of the valve metal oxide on the properties of ruthenium based mixed oxide electrodes: II. RuO2/TiO2 coatings. J Electrochem Soc. 1989;136:2596–8.

75. Kim KW, Lee EH, Kim JS, Shin KH, Kim KH. Effect of an etching Ti substrate on a catalytic oxide electrode. J Electrochem Soc. 2001;148(3):111.

76. Marcu M, Preda L, Vizireanu S, Bita B, Mihai MA, Spataru T, et al. Enhancement of the capacitive features of WO3 supported on pristine and functionalized graphite by appropriate adjustment of the electrodeposition regime. Materials Science and Engineering: B. 2022 Mar;277:115585.

77. Antonczak AJ, Skowronski L, Trzcinski M, Kinzhybalo VV, Lazarek LK, Abramski KM. Laser-induced oxidation of titanium substrate: analysis of the physicochemical structure of the surface and sub-surface layers. Appl Surf Sci. 2015;325:217–26.

78. Vasilaki E, Vernardou D, Kenanakis G, Vamvakaki M, Katsarakis N. TiO2/WO3 photoactive bilayers in the UV–Vis light region. Appl Phys A. 2017;123:231.

79. Chew YH, Tang JY, Tan LJ, Choi BWJ, Tan LL, Chai SP. Engineering surface oxygen defects on tungsten oxide to boost photocatalytic oxygen evolution from water splitting. Chem Commun. 2019;55(44):6265–8.

80. Wei Z, Wang W, Li W, Bai X, Zhao J, Tse ECM, et al. Steering electron–hole migration pathways using oxygen vacancies in tungsten oxides to enhance their photocatalytic oxygen evolution performance, Angew. Chem Int Ed. 2021;60(15):8236–42.

81. Sojjad AKL, Shamaila S, Tian B, Chen F, Zhang J. One step activation of WOx/TiO2 nanocomposites with enhanced photocatalytic activity. Appl Catal B: Environ. 2009;91:397–405.

82. Kong M, Li Y, Chen X, Tian T, Fang P, Zheng F, et al. Tuning the relative concentration ratio of bulk defects to surface defects in TiO2 nanocrystals leads to high photocatalytic efficiency. J Am Chem Soc. 2011;133(41):16414–7.

83. Li X, Liu H, Sun Y, Zhu L, Yin X, Sun S, et al. High oxygen evolution activity of tungsten bronze oxides boosted by anchoring of Co2+ at Nb5+ sites accompanied by substantial oxygen vacancy. Adv Sci. 2020;7:2002242.

84. Iandolo B, Zhang H, Wickman I, Zorić I, Conibeer G, Hellman A. Correlating flat band and onset potentials for solar water splitting on model hematite photoanodes. RSC Adv. 2015;5(75):61021–30.

85. Reichert R, Zambrzycki C, Jusys Z, Behm RJ. Photo-electrochemical oxidation of organic C1 molecules over WO3 films in aqueous electrolyte: Competition between water oxidation and C1 oxidation. ChemSusChem. 2015;8:3677–87.

86. Zeng Q, Bai J, Li J, Li L, Xia L, Zhou B, et al. Highly-stable and efficient photocatalytic fuel cell based on the epitaxial TiO2/WO3/W nanothorn photoanode and enhanced radical reactions for simultaneous electricity production and wastewater treatment. Appl Energy. 2018;220:127–37.

87. Yuda A, Ashok A, Kumar A. A comprehensive and critical review on recent progress in anode catalyst for methanol oxidation reaction. Catal Rev. 2022;64(1):126–228.

88. Qiu M, Sun P, Shen L, Wang K, Song S, Yu X, et al. WO_3 nanoflowers with excellent pseudo-capacitive performance and the capacitance contribution analysis. J Mater Chem A. 2016;4(19):7266–73.

89. Simon P, Gogotsi Y, Dunn B. Where Do Batteries End and Supercapacitors Begin? Science. 2014 Mar 14;343(6176):1210–1.

90. Brousse T, Bélanger D, Long JW. To Be or Not To Be Pseudocapacitive? J Electrochem Soc. 2015;162(5):A5185–9.

91. Guerra A, Achour A, Vizireanu S, Dinescu G, Messaci S, Hadjersi T, et al. ZnO/Carbon nanowalls shell/core nanostructures as electrodes for supercapacitors. Applied Surface Science. 2019 July;481:926–32.

92. Zarshad N, Wu J, Rahman AU, Tariq M, Ali A, Ni H. MnO2 nanospheres electrode composed of low crystalline ultra-thin nanosheets for high performance and high rate supercapacitors. Materials Science and Engineering: B. 2020 Sept;259:114610.

93. Xiao X, Li S, Wei H, Sun D, Wu Y, Jin G, et al. Synthesis and characterization of VO2(B)/graphene nanocomposite for supercapacitors. J Mater Sci: Mater Electron. 2015 June;26(6):4226–33.

94. Stoica SD, Vizireanu S, Acsente T, Dinescu G. Hybrid Nanomaterial Architectures: Combining Layers of Carbon Nanowalls, Nanotubes, and Particles. Plasma Chem Plasma Process. 2018 July;38(4):695–706.

95. Kaipannan S, Marappan S. Fabrication of 9.6 V High-performance Asymmetric Supercapacitors Stack Based on Nickel Hexacyanoferrate-derived Ni(OH)2 Nanosheets and Bio-derived Activated Carbon. Sci Rep. 2019 Jan 31;9(1):1104.

96. Li M, Liu D, Wei D, Song X, Wei D, Wee ATS. Controllable Synthesis of Graphene by Plasma-Enhanced Chemical Vapor Deposition and Its Related Applications. Advanced Science. 2016 Nov;3(11):1600003.

97. González Z, Vizireanu S, Dinescu G, Blanco C, Santamaría R. Carbon nanowalls thin films as nanostructured electrode materials in vanadium redox flow batteries. Nano Energy. 2012 Nov;1(6):833–9.

98. Yan J, Liu J, Fan Z, Wei T, Zhang L. High-performance supercapacitor electrodes based on highly corrugated graphene sheets. Carbon. 2012 May;50(6):2179–88.

99. Sun P, Deng Z, Yang P, Yu X, Chen Y, Liang Z, et al. Freestanding CNT–WO_3 hybrid electrodes for flexible asymmetric supercapacitors. J Mater Chem A. 2015;3(22):12076–80.

100. Shen Y, Yamazaki T, Liu Z, Meng D, Kikuta T, Nakatani N. Influence of effective surface area on gas sensing properties of WO3 sputtered thin films. Thin Solid Films. 2009 Jan;517(6):2069–72.

101. Baeck S -H., Choi K -S., Jaramillo TF, Stucky GD, McFarland EW. Enhancement of Photocatalytic and Electrochromic Properties of Electrochemically Fabricated Mesoporous WO_3 Thin Films. Advanced Materials. 2003 Aug 5;15(15):1269–73.

102. Chu J, Lu D, Wang X, Wang X, Xiong S. WO3 nanoflower coated with graphene nanosheet: Synergetic energy storage composite electrode for supercapacitor application. Journal of Alloys and Compounds. 2017 Apr;702:568–72.

103. White CM, Gillaspie DT, Whitney E, Lee SH, Dillon AC. Flexible electrochromic devices based on crystalline WO3 nanostructures produced with hot-wire chemical vapor deposition. Thin Solid Films. 2009 Apr;517(12):3596–9.

104. Spătaru T, Preda L, Osiceanu P, Munteanu C, Anastasescu M, Marcu M, et al. Role of surfactant-mediated electrodeposited titanium oxide substrate in improving electrocatalytic features of supported platinum particles. Applied Surface Science. 2014 Jan;288:660–5.

105. Spătaru T, Osiceanu P, Munteanu C, Spătaru N, Fujishima A. Electrochemical preparation and characterization of a cobalt oxide–platinum composite with promising capacitive and electrocatalytic features. J Solid State Electrochem. 2012 Dec;16(12):3897–905.

106. Vijayakumar E, Yun YH, Quy VHV, Lee YH, Kang SH, Ahn KS, et al. Development of Tungsten Trioxide Using Pulse and Continuous Electrodeposition and Its Properties in Electrochromic Devices. J Electrochem Soc. 2019;166(4):D86–92.

107. Cai G, Cui M, Kumar V, Darmawan P, Wang J, Wang X, et al. Ultra-large optical modulation of electrochromic porous WO_3 film and the local monitoring of redox activity. Chem Sci. 2016;7(2):1373–82.

108. Mihai S, Cursaru D, Matei D, Dinescu A, Stoica SD, Sorin V, et al. Carbon nanowalls decorated with gold nanoparticles for surface-enhanced raman spectroscopy. Digest Journal of Nanomaterials and Biostructures. 2018 July 1;13:743–9.

109. Stoica SD, Vizireanu S, Luculescu CR, Mitu B, Dinescu G. Metastable growth regime for carbon nanowalls and carbon nanofibers in an $Ar/H_2/C_2H_2$ radiofrequency plasma jet. Plasma Sources Sci Technol. 2020 Oct 1;29(10):105007.

110. Vizireanu S, Mitu B, Luculescu CR, Nistor LC, Dinescu G. PECVD synthesis of 2D nanostructured carbon material. Surface and Coatings Technology. 2012 Oct;211:2–8.

111. Vizireanu S, Stoica SD, Luculescu C, Nistor LC, Mitu B, Dinescu G. Plasma techniques for nanostructured carbon materials synthesis. A case study: carbon nanowall growth by low pressure expanding RF plasma. Plasma Sources Sci Technol. 2010 June 1;19(3):034016.

112. Pauporté T. A Simplified Method for WO[sub 3] Electrodeposition. J Electrochem Soc. 2002;149(11):C539.

113. Vasilopoulou M, Soultati A, Georgiadou DG, Stergiopoulos T, Palilis LC, Kennou S, et al. Hydrogenated under-stoichiometric tungsten oxide anode interlayers for efficient and stable organic photovoltaics. J Mater Chem A. 2014;2(6):1738–49.

114. Ion R, Vizireanu S, Stancu CE, Luculescu C, Cimpean A, Dinescu G. Surface plasma functionalization influences macrophage behavior on carbon nanowalls. Materials Science and Engineering: C. 2015 Mar;48:118–25.

115. Dias P, Lopes T, Andrade L, Mendes A. Temperature effect on water splitting using a Si-doped hematite photoanode. Journal of Power Sources. 2014 Dec;272:567–80.

116. Hu G, Li J, Liu P, Zhu X, Li X, Ali RN, et al. Enhanced electrocatalytic activity of WO3@NPRGO composite in a hydrogen evolution reaction. Applied Surface Science. 2019 Jan;463:275–82.

117. Zheng JP, Jow TR. A New Charge Storage Mechanism for Electrochemical Capacitors. J Electrochem Soc. 1995 Jan 1;142(1):L6–8.

118. Spătaru N, Zhang X, Spătaru T, Tryk DA, Fujishima A. Anodic Deposition of RuO[sub x]·nH[sub 2]O at Conductive Diamond Films and Conductive Diamond Powder for Electrochemical Capacitors. J Electrochem Soc. 2008;155(1):D73.

119. Stoller MD, Park S, Zhu Y, An J, Ruoff RS. Graphene-Based Ultracapacitors. Nano Lett. 2008 Oct 8;8(10):3498–502.

120. Hung TC, Chen CF, Whang WT. Deposition of Carbon Nanowall Flowers on Two-Dimensional Sheet for Electrochemical Capacitor Application. Electrochem Solid-State Lett. 2009;12(6):K41.

121. Yamanaka K, Oakamoto H, Kidou H, Kudo T. Peroxotungstic Acid Coated Films for Electrochromic Display Devices. Jpn J Appl Phys. 1986 Sept 1;25(9R):1420.

122. Vatamanu J, Borodin O, Olguin M, Yushin G, Bedrov D. Charge storage at the nanoscale: understanding the trends from the molecular scale perspective. J Mater Chem A. 2017;5(40):21049–76.

123. Bard AJ, Faulkner LR. Electrochemical Methods: Fundamentals and Applications. Ediția a II-a. New York, SUA: John Wiley & Sons, Inc.; 2000.

124. Marcu M, Spataru T, Calderon-Moreno JM, Osiceanu P, Preda L, Spataru N. Anodic Voltammetry of Epinephrine at Graphene-Modified Conductive Diamond Electrodes and Its Analytical Application. J Electrochem Soc. 2018;165(11):B523–9.

125. Vizireanu S, Ionita MD, Ionita RE, Stoica SD, Teodorescu CM, Husanu MA, et al. Aging phenomena and wettability control of plasma deposited carbon nanowall layers. Plasma Process Polym. 2017 Nov;14(11):1700023.

126. Wang PH, Wang TL, Lin WC, Lin HY, Lee MH, Yang CH. Enhanced Supercapacitor Performance Using Electropolymerization of Self-Doped Polyaniline on Carbon Film. Nanomaterials. 2018 Mar 31;8(4):214.

127. Amatucci GG, Badway F, Du Pasquier A, Zheng T. An Asymmetric Hybrid Nonaqueous Energy Storage Cell. J Electrochem Soc. 2001;148(8):A930.